Simple *b* Ions Have Cyclic Oxazolone Structures. A Neutralization-Reionization Mass Spectrometric and Computational Study of Oxazolone Radicals

Xiaohong Chen and František Tureček
Department of Chemistry, University of Washington, Seattle, Washington, USA

The 2-methyloxazol-5-on-2-yl radical (**3**) and its deuterium labeled analogs were generated in the gas-phase by femtosecond electron-transfer and studied by neutralization-reionization mass spectrometry and quantum chemical calculations. Radical **3** undergoes fast dissociation by ring opening and elimination of CO and CH_3CO. Loss of hydrogen is less abundant and involves hydrogen atoms from both the ring and side-chain positions. The experimental results are corroborated by the analysis of the potential energy surface of the ground electronic state in **3** using density functional, perturbational, and coupled-cluster theories up to CCSD(T) and extrapolated to the 6-311 ++ G(3df,2p) basis set. RRKM calculations of radical dissociations gave branching ratios for loss of CO and H that were $k_{CO}/k_H > 10$ over an 80–300 kJ mol^{-1} range of internal energies. The driving force for the dissociations of **3** is provided by large Franck-Condon effects on vertical neutralization and possibly from involvement of excited electronic states. Calculations also provided the adiabatic ionization energy of **3**, IE_{adiab} = 5.48 eV and vertical recombination energy of cation $\mathbf{3}^+$, RE_{vert} = 4.70 eV. The present results strongly indicate that oxazolone structures can explain fragmentations of ***b***-type peptide ions upon electron capture, contrary to previous speculations. (J Am Soc Mass Spectrom 2005, 16, 1941–1956) © 2005 American Society for Mass Spectrometry

Upon low-energy collisions, gas-phase peptide ions fragment by peptide bond cleavages that result in the formation of ions containing N-terminal residues (***b***-series ions) and C-terminal residues (***y***-ion series) [1]. Based on both ion dissociations and computational studies of ion structure and energetics, it is generally accepted that ***y*** ions correspond to truncated protonated peptides [2]. In contrast, there has been some recent disagreement regarding ***b*** ions for which as many as four different structures have been proposed, e.g., (*1*) open chain acylium; (*2*) protonated oxazolone; (*3*) protonated diketopiperazine; and (*4*) immonium ions formed from oxazolone structures [3]. Quantum chemical calculations at various levels of theory (Hartree-Fock, Møller-Plesset, and density functional theory) prefer protonated oxazolone structures for ***b***-ions that are usually the most stable or the only stable isomers [4, 5]. The formation of protonated oxazolone structure for ***b***-ions is also consistent with the mechanism of peptide ion dissociations that was elucidated by detailed ab initio calculations on model di- and tripeptides [6], as discussed in detail in a recent authoritative review [3]. The fragmentation mechanism (Scheme **1**) involves proton migration to the amide nitrogen followed by a nucleophilic attack at the amide carbonyl by the neighboring carbonyl oxygen from the N-terminal site. This forms an intermediate with an N-protonated oxazolone ring that can eliminate a molecule of the neutral C-terminal-truncated peptide to form the ***b***-ion [4]. Alternative structures and mechanisms for ***b***-ion formation have been proposed for peptides having polar groups in side chains of amino acid residues, His, Glu, Asn, Lys, and Arg, if these were at N-terminal sites of the peptide bond to be cleaved [7].

Experimental support for oxazolone ***b***-ion structures was provided by CAD spectra of model systems. For example, Yalcin et al. showed that the CAD spectrum of the ***b*** ion from protonated C_6H_5CO—Gly-Gly-OH matched that of protonated 2-phenyloxazol-5-one [4]. The reported low-energy CAD spectra showed only two fragment ions due to loss of CO and formation of $C_6H_5CO^+$ [4]. Evidence for oxazolone-like *neutral counterparts* of ***y***-type ions was provided by the collisional-reionization spectrum of neutral fragments eliminated from protonated C_6H_5CO—Gly-Phe-OH that was similar to that of the neutralization-reionization mass spectrum of authentic 2-phenyloxazol-5-one cation-radical [8].

However, new questions about ***b***-ion structure have been raised recently by Haselmann and coworkers who

Published online October 28, 2005

Address reprint requests to Dr. F. Tureček, Department of Chemistry, University of Washington, Bagley Hall, Box 351700, Seattle, WA 98195-1700, USA. E-mail: turecek@chem.washington.edu

1044-0305/05/$30.00
doi:10.1016/j.jasms.2005.07.023

Received June 24, 2005
Revised July 27, 2005
Accepted July 27, 2005

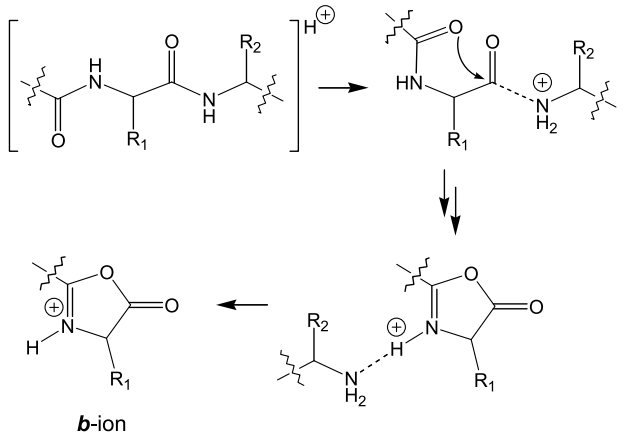

Scheme 1

observed a loss of CO upon electron-capture dissociation (ECD) of doubly charged ***b*** ions from several peptides. These authors hypothesized on the basis of their findings that the ***b***-ions might have open-chain acylium structures because only those could be expected to eliminate CO from acyl radicals produced by electron-capture neutralization [9]. In contrast, Haselmann et al. argued that elimination of CO from cyclic oxazolone radicals would be energetically unfavorable.

We decided to test the Haselmann hypothesis by generating authentic oxazolone radicals and study their unimolecular dissociations by neutralization-reionization mass spectrometry (NRMS) [10]. NRMS relies on the generation of gas-phase ions of well-defined structures that are separated by mass, accelerated to a high velocity (typically 100,000–200,000 ms^{-1} at kinetic energies in the 5–10 keV range), and discharged by a glancing collision with a gaseous neutral target [11]. For neutralization of cations, collisional electron-transfer from a thermal neutral donor, which is usually a polarizable molecule such as CH_3SSCH_3, $(CH_3)_3N$, N,N-dimethylaniline, etc., occurs on a time scale of a few femtoseconds to form the transient neutral species [12]. This ultrashort time scale for the electron-transfer guarantees that the incipient fast neutral has the structure of the ion precursor. In addition, the use of polarizable "soft" targets minimizes collisionally activated dissociation of the ions sampled for neutralization [12]. The fast neutrals are separated from the residual ions, allowed a few microseconds to dissociate, and the mixture of surviving neutral species and their dissociation products is non-selectively ionized to provide a NR mass spectrum. The latter provides a practically complete analysis of all dissociation products originating from the transient neutral intermediate [13]. In addition, ion activation in the ionizing collision can result in ion dissociations whose charged products also appear in the NR mass spectrum. Products of neutral and post-reionization ion dissociations can be distinguished by chemical or instrumental means. The former are applicable when the collision-induced and NR dissociations of the given ion substantially differ to be readily distinguished in the NR mass spectra. Instrumental methods for distinguishing ion and neutral dissociations rely on neutral photoexcitation [14], or variable-time measurements [15].

In our approach, simple ***b***-ions were represented by N-protonated 2-methyl-1,3-oxazol-5-one, $\mathbf{3}^+$, which we generated from 2-methyl-1,3-oxazol-one (**1**) and which was proved to possess a cyclic structure. Cation $\mathbf{3}^+$ was converted to radical **3** by collisional electron-transfer for studies of radical dissociations. To elucidate dissociation mechanisms, we used deuterium-labeled derivatives $\mathbf{3a}^+$ and $\mathbf{3b}^+$ that were converted to the corresponding radicals **3a** and **3b**, respectively.

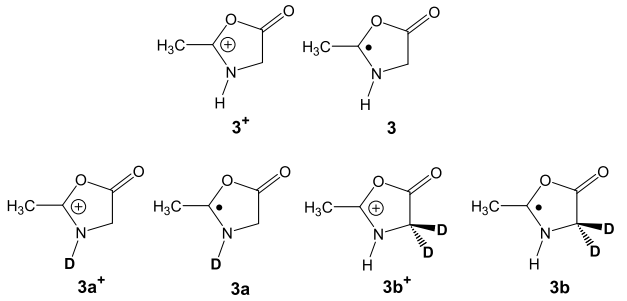

Structure 1

The experimental results were complemented by ab initio calculations at high levels of theory to provide reaction and transition-state energies for radical **3**. The transition-state energies were further used to perform Rice-Ramsperger-Kassel-Marcus (RRKM) [16] calculations of rate constants to obtain branching ratios for radical dissociations.

Experimental

Materials

Dimethyl disulfide (DMDS, 98%), N-acetylglycine (99%), ethyl choloroformate (97%), *p*-toluenesulfonic acid monohydrate (99%), and sulfuric acid-d_2 (98 wt % solution in D_2O, 99.5+ atom% D) were purchased from Sigma-Aldrich (Milwaukee, WI). Ammonia-d_3 (99 atom% D), glycine-2,2-d_2 (98 atom% D), methanol-d_4 (99.8 atom % D), and D_2O (99.9 atom % D) were purchased from Cambridge Isotope Laboratories, Inc. (Andover, MA). Triethylamine (TEA) (98%) was purchased from J. T. Baker, Inc. (Phillipsburg, NJ). All the compounds were used as received.

2-Methyloxazol-5-One **(1)**. To a stirred mixture of N-acetylglycine (5 g, 4.3 mmol) and triethylamine (5.2 g, 5.1 mmol) in 125 mL of dry benzene was added ethyl choloroformate (5.1 g, 4.7 mmol) and the mixture was then stirred at room-temperature for 3 h [17]. The precipitated triethylamine hydrochloride was filtered off, the filtrate was evaporated, and the residue was

purified by short-path vacuum distillation at 0.5 torr. GC mass spectrum: *m/z* (% relative intensity): 99 (35), 82 (6), 71 (63), 54 (13), 44 (11), 43 (100), 42 (11), 29 (92), 28 (40), 27 (45), 15 (8). ^{1}H-NMR ($CDCl_3$): 2.40 (s, 3H, CH_3), 4.39 (s, 2H, CH_2).

N-Acetylglycine Ethyl Ester **(2)**. N-acetylglycine (5 g) and *p*-toluenesulfonic acid monohydrate (170 mg) were dissolved in 170 mL of anhydrous ethanol and the solution was refluxed for 6 h. The solution was then cooled, the solvent was evaporated in vacuo, and the residue was dissolved in 170 mL chloroform, and washed with 2 × 20 mL 5 wt % sodium bicarbonate. The chloroform solution was dried with anhydrous sodium sulfate, filtered, the solvent was evaporated, and the product was purified by vacuum distillation. GC mass spectrum: *m/z* (% relative intensity): 145 (1), 100 (5), 99 (6), 73 (13), 72 (48), 43 (58), 42 (9), 30 (100), 29 (22), 28 (20), 15 (8).

N-Acetylglycine-2,2-d_2 **(1b)**. Glycine-2,2-d_2 (5 g) was dissolved in 34 mL of 2M NaOD in D_2O and acetic anhydride (13 g) was added under stirring and cooling followed by another 125 mL of 2M NaOD [18]. After 20 min. the mixture was acidified with 32 mL of 5M D_2SO_4 in D_2O, and the aqueous layer was extracted with 6 × 40 mL of ethyl acetate. The organic extract was dried with anhydrous Na_2SO_4, filtered, and the solvent was evaporated in vacuo to yield 2.8 g (36%) of a crystalline product.

2-methyl-1,3-oxazol-5-one-4,4-d_2 **(1b)**. Prepared from N-acetylglycine-2,2-d_2 as described for **1**. GC mass spectrum: *m/z* (% relative intensity): 101 (2), 100 (36), 99 (7), 83 (7), 73 (3), 72 (70), 71 (13), 55 (16), 44 (21), 43 (100), 42 (18). ^{1}H-NMR ($CDCl_3$): 2.38 (s, 3H, CH_3).

N-Acetylglycine ethyl ester-N-d **(2a)**. Prepared by H/D transmittance exchange of the labile proton in **2** (0.3 g) by stirring in CD_3OD (0.8 mL) for 3 h and evaporating the solvent in vacuo. The crude product was used for mass spectrometric measurements without further purification. Mass spectrum: *m/z* (% relative intensity): 147 (32), 102 (14), 100 (3.5), 75 (26), 74 (76), 43 (32), 32 (100), 29 (8).

Methods

Neutralization-reionization (NR) mass spectra were measured on a tandem quadrupole acceleration-deceleration mass spectrometer described previously [19]. Ions were generated in the gas-phase in standard electron impact (EI) or chemical ionization (CI) ion sources [12].°The°source°conditions°were°as°follows:°emission current, 500 μA for EI and 1 mA for CI. The electron energy was tuned for the best signal but typically was 70 eV for EI and 100 eV for CI. The source temperature was 200–220 °C. Liquid samples were degassed by several freeze-pump-thaw cycles and introduced into the ion source from a glass liquid probe at room-temperature. Due to its high volatility, the triethylamine probe was kept at 0°C throughout each experimental period to keep the pressure stable. NH_3 and ND_3 were used as CI reagent gases at pressures $8.0–9.0 \times 10^{-5}$ torr as read on an ionization gauge located at the diffusion pump intake. The ions were extracted from the source, transmitted through a radio-frequency-only quadrupole filter, accelerated to 7250 eV and focused on a collision cell floated at −7170 V, where dimethyldisulfide vapor was admitted at pressures such as to achieve 70% ion beam transmission. According to Poisson statistics, out of the 30% ions that underwent collisions 83% collided only once. Residual ions and neutrals were allowed to drift to a four-segment conduit maintained at +250 V that reflected the ions while allowing the neutrals to pass through. The neutral drift time was 5.1 μs for species of 100 Da mass. The neutrals were non-selectively reionized by collisions with oxygen at pressures allowing 70% beam transmittance. The ions formed then were decelerated to 75–80 eV, energy filtered, and analyzed by a quadrupole mass filter that was operated at unit mass resolution.

The quadrupole analyzer and the deceleration voltage were scanned in link to allow transmission of ions of mass m_f that have kinetic energies (eV_f) according to eq 1, where m_p is the precursor ion mass and V_p is the acceleration°potential°[19].

$$V_f = V_p \frac{m_f}{m_p} \quad (1)$$

In case that there are precursor ions at adjacent masses (m_{p1} and m_{p2}) forming a common fragment m_f, the latter is transmitted through the energy filter lens if the difference in the product ion kinetic energies (ΔeV) is comparable to or smaller than the filter energy bandpass width $\Delta T_{pass} \approx$ 40°eV°(eq°2)°[19].°For°example,°product°ions°at°*m/z* 57 produced from 7-keV precursor ions of *m/z* 100 and 101 will have (ΔeV) = 40 eV and thus be transmitted and appear in the NR mass spectrum at *m/z* 57.

$$\Delta(eV) = eV_p m_f \left| \frac{1}{m_{p1}} - \frac{1}{m_{p2}} \right| \leq \Delta T_{pass} \quad (2)$$

The instrument was tuned daily to match the reference NR mass spectrum of CS_2. Typically, 50 repetitive scans were accumulated per spectrum at a 1 mass unit/s scan rate, corresponding to 200 data points per peak.

^{1}H-NMR spectra were measured on an Bruker Avance 300 spectrometer at 300.13 MHz in $CDCl_3$ at 25°C. Gas-chromatography mass spectrometry was performed on an HP 5971A instrument equipped with a silicone elastomer DB5 GC capillary column. Electron impact and chemical ionization mass spectra were measured on a JEOL HX-110 double focusing instrument equipped with EI and CI ion sources. Samples were introduced from a direct probe at 50 °C. Triethylamine was introduced from a gas reservoir. Collisionally activated dissociation (CAD) spectra were

measured on the JEOL HX-110 instrument by scanning the electrostatic (E) and magnet (B) analyzers while maintaining a constant B/E ratio (B/E linked scan). Air as the collision gas was admitted to the first field-free region at pressures to achieve 50 and 70% beam transmittance at 10 keV. Typically 20–30 scans were collected and averaged. The low ΔT_{pass} of the electrostatic analyzer (<2 eV) and high ion kinetic energy secured that precursor ions at adjacent masses were completely separated throughout the entire mass range of *m/z* 10–103.

Calculations

Standard ab initio and density functional theory calculations were performed using the Gaussian 03 suite of programs [20]. Geometries were optimized with Becke's hybrid functional (B3LYP) [21] using the 6-31++G(d,p) basis set. The Supplementary Material section containing tables of optimized geometries (cartesian coordinate formate, standard orientation) can be accessed in the electronic version of this article. The same level of theory was used for frequency analysis to characterize local energy minima (all real frequencies) and transition states as first-order saddle points (one imaginary frequency). Improved energies were obtained by single-point calculations using B3LYP and Møller-Plesset theory [22] truncated at second-order (MP2, frozen core) and the larger triple-ζ split valence 6-311 ++ G(3df,2p) basis set furnished with multiple shells of polarization functions at C, N, O, and H, one shell of diffuse s and p functions at C, N, and O, and one shell of diffuse s functions at H. Spin unrestricted calculations (UB3LYP and UMP2) were performed for open-shell systems. Spin contamination was negligible in UB3LYP computations, as evidenced by the expectation values of the spin operator that were all $\langle S^2 \rangle \leq 0.76$. UMP2 energies were corrected by spin projection [23] (PMP2) that lowered $\langle S \rangle$ to ≤ 0.76 and resulted in 6.7 millihartree energy corrections (root mean square deviation). The B3LYP and MP2 or PMP2 single point energies were averaged according to the previously reported B3-MP2 scheme [24] that has been shown to achieve improved accuracy at the level of highly correlated composite ab initio methods by canceling small errors inherent to the B3LYP and MP2 approximations [25]. Another set of energies was obtained for selected species from single point calculations with coupled cluster theory [26] employing single, double and disconnected triple excitations of valence electrons [27], CCSD(T), and the 6-311G(d,p) basis set. The energies were extrapolated to CCSD(T)/6-311 + G(2d,p) and CCSD(T)/6-311 ++ G(3df,2p) using standard linear formulas, eq 3 and 4 [28].

$$E[\mathrm{CCSD(T)/6\text{-}311{+}G(2d,p)}] \approx E[\mathrm{CCSD(T)/6\text{-}311G(d,p)}] + E[\mathrm{MP2/6\text{-}311{+}G(2d,p)}] - E[\mathrm{MP2/6\text{-}311G(d,p)}] \quad (3)$$

$$E[\mathrm{CCSD(T)/6\text{-}311{+}{+}G(3df,2p)}] \approx E[\mathrm{CCSD(T)/6\text{-}311G(d,p)}] + E[\mathrm{MP2/6\text{-}311{+}{+}G(3df,2p)}] - E[\mathrm{MP2/6\text{-}311G(d,p)}] \quad (4)$$

These effective CCSD(T) calculations gave similar relative energies for the species under study, and so only results from the larger basis set expansion (eq 4) are reported here. The B3-MP2 and CCSD(T) energies were used to calculate relative energies that were corrected for zero-point vibrational contributions. The reported relative energies thus correspond to 0 K unless stated otherwise. Enthalpy corrections and entropies were calculated from B3LYP/6-31 ++ G(d,p) harmonic frequencies and moments of inertia within the rigid rotor-harmonic oscillator approximation. Complete active space (CASSCF) [29] calculations were carried out to investigate selected dissociation pathways and used the 6-31 ++ G(d,p) basis set.

RRKM calculations were performed using Hase's program [30] that was recompiled and run under Windows XP [31]. Direct count of quantum states was used in 2 kJ mol^{-1} steps from the transition-state energy up to 300 kJ mol^{-1} above it. Rotational states were treated adiabatically. The calculated microscopic rate constants, $k(E,J,K)$, were Boltzmann averaged over the rotational states at 473 K, corresponding to the ion source temperature that defines the precursor ion rotational temperature, to give microcanonical rate constants $k(E)$.

Results and Discussion

Ion Formation and Dissociations

A logical pathway to generate ion $\mathbf{3}^+$ is by selective protonation of a cyclic neutral precursor, 2-methyl-1,3-oxazol-5-one (**1**). Combined MP2 and B3LYP/6-311 ++ G(3df,2p) and CCSD(T) calculations of the topical proton affinities (PA) in **1** point to N-3 as the most basic site of PA = 877 kJ mol^{-1}. The O-1 (PA = 791 kJ mol^{-1}) and O-6 (PA = 736 kJ mol^{-1}) positions are substantially less basic. These features allowed us to use NH_4^+ as a gas-phase acid (PA(NH_3) = 854 kJ mol^{-1}) [32] for mildly exothermic and selective protonation of **1** at N-3 to form the desired ion $\mathbf{3}^+$. Protonations with NH_4^+ at positions O-1 and O-6 in **1** are endothermic and therefore both kinetically [33] and thermodynamically disfavored under chemical ionization conditions in the gas phase [34]. CI-NH_3 of **1** formed the desired ion $\mathbf{3}^+$ at *m/z* 100 that was characterized by accurate mass measurements (measured 100.0393, $C_4H_6NO_2$ requires 100.0398) and CAD mass spectra, as described below.

Another route to ion $\mathbf{3}^+$ or its isomers is by dissociative ionization with 70-eV electrons of an acyclic precursor, N-acetylglycine ethyl ester, that eliminates OC_2H_5 to produce a $C_4H_6NO_2^+$ ion at *m/z* 100 that was also characterized by accurate mass measurements and CAD mass spectra. This ion is denoted as $\mathbf{3'}^+$. The loss of OC_2H_5 is accompanied by an elimination of C_2H_5OH that produces a $C_4H_5NO_2^{+\cdot}$ ion at the adjacent *m/z* 99.

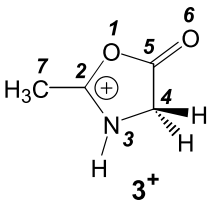

Structure 2

We also prepared deuterium-labeled derivatives of $\mathbf{3}^+$ and characterized them by accurate mass measurements and CAD spectra. The N-D labeled ion $\mathbf{3a}^+$ (*m/z* 101) was prepared by ND_3/CI of **1**. The 4,4-D_2 labeled ion $\mathbf{3b}^+$ was prepared by NH_3/CI of **1b**. N-D and 4,4-D_2 analogs $\mathbf{3a'}^+$ and $\mathbf{3b'}^+$ were also prepared by 70-eV dissociative ionization of N-D-acetylglycine ethylester and N-acetyl-2,2-D_2-glycine ethyl ester, respectively.

The CAD spectra of $\mathbf{3}^+$ and $\mathbf{3'}^+$ show similar dissociations (Figure 1). Unimolecular dissociations of metastable $\mathbf{3}^+$ and $\mathbf{3'}^+$ proceed by elimination of CO to give the *m/z* 72 fragment ions that are also abundant in the CAD spectra. The other collision-induced dissociations of $\mathbf{3}^+$ and $\mathbf{3'}^+$ are loss of H (*m/z* 99), loss of CO + CH_3 (*m/z* 57), and the formation of CH_3CO^+ (*m/z* 43) and $CH_2 = NH_2^+$ (*m/z* 30). The substantially greater relative abundance of the $(M - CO)^+$ ion from $\mathbf{3'}^+$ can be accounted for by a higher fraction of metastable ions produced by electron impact-induced dissociation of the N-acetylglycine ester precursor, compared to the metastable fraction of $\mathbf{3}^+$ generated under CI conditions by mildly exothermic proton transfer. Other than the *m/z* 72 ion relative intensity, the CAD spectra of $\mathbf{3}^+$ and $\mathbf{3'}^+$ are practically identical.

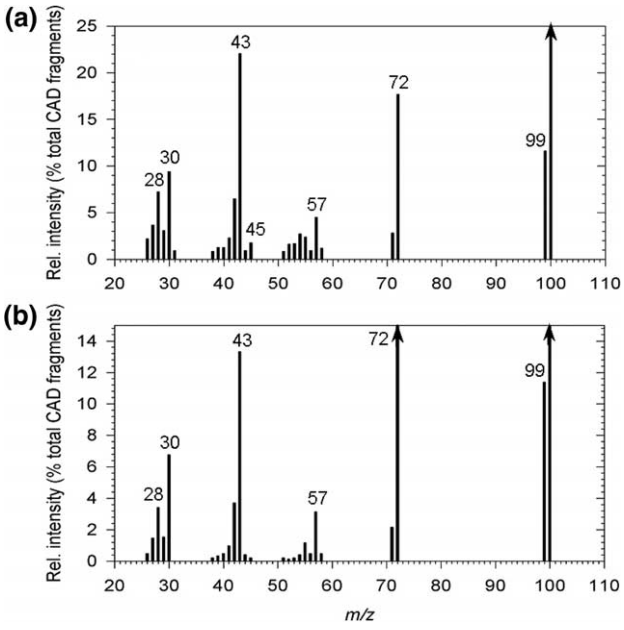

Figure 1. 10-keV CAD mass spectra of (**a**) ion $\mathbf{3}^+$ from CI-NH_3 protonation of 2-methyloxazol-5-one, and (**b**) ion $\mathbf{3'}^+$ from dissociative ionization of N-acetylglycine ethyl ester. The peaks denoted by arrows are truncated on the relative intensity scale.

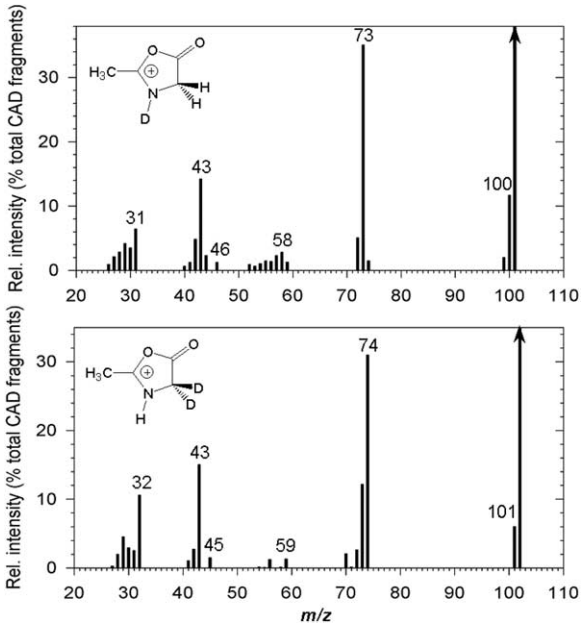

Figure 2. 10-keV CAD mass spectra of (top) ion $\mathbf{3a}^+$ and (bottom) ion $\mathbf{3b}^+$. The peaks of precursor ions denoted by arrows are truncated on the relative intensity scale.

Deuterium labeling in $\mathbf{3a}^+$ and $\mathbf{3b}^+$ manifests itself by mass shifts in the pertinent CAD mass spectra (Figure 2). Both $\mathbf{3a}^+$ and $\mathbf{3b}^+$ show mainly loss of a light hydrogen atom, indicating that the latter originates from the exocyclic methyl group to form a 2-methylene-1,3-oxazolin-5-one cation-radical ($\mathbf{7}^{+\cdot}$) (Scheme **2**). Eliminations of CO and CO + CH_3 show retention of the deuterium label in the fragment ions, as corroborated by the relevant mass shifts in the CAD spectra (*m/z* 73 and 58 from $\mathbf{3a}^+$ and *m/z* 74 and 59 from $\mathbf{3b}^+$). The acetyl ion at *m/z* 43 does not contain deuterium when formed from $\mathbf{3a}^+$ and $\mathbf{3b}^+$. The mass shifts *m/z* 30 → *m/z* 31 and *m/z* 30 → *m/z* 32 for $\mathbf{3a}^+$ and $\mathbf{3b}^+$, respectively, indicate that the $CH_2 = NH_2^+$ cations incorporate the N-3—C-4 moiety that receives a hydrogen atom from the methyl group in the course of dissociation.

The facile elimination of CO from $\mathbf{3}^+$ is consistent with the energetics of this dissociation that has been

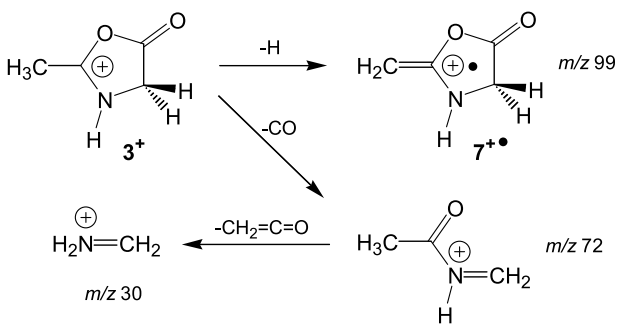

Scheme 2

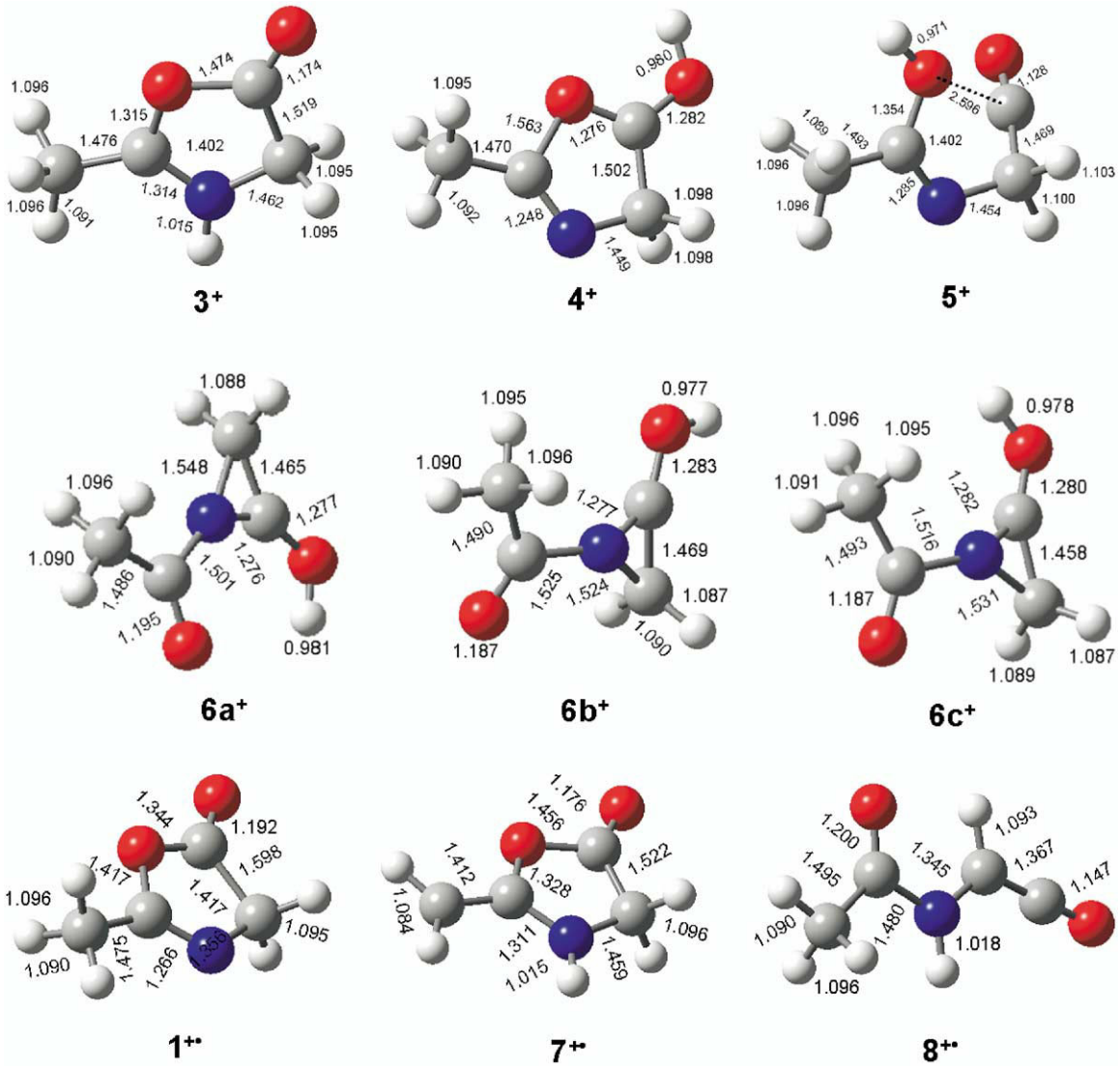

Figure 3. B3LYP/6-31 ++ G(d,p) optimized structures of ions $\mathbf{3}^+$,$\mathbf{4}^+$, $\mathbf{5}^+$, $\mathbf{6a}^+$–$\mathbf{6c}^+$, $\mathbf{1}^{+\cdot}$, $\mathbf{7}^{+\cdot}$, and $\mathbf{8}^{+\cdot}$. Bond lengths in angstroms.

shown to occur in a variety of peptide ***b*** ions and was calculated to require low activation energies (113–119 kJ mol^{-1})°in°related°oxazolone°cations°[6].

Ion Structures and Dissociation Energetics

The ion dissociations observed upon CAD can be related to the ion relative stabilities and dissociation energies. We obtained by DFT calculations several ion structures that were local energy minima, as shown in Figure°3.°N-protonated°oxazolone°$\mathbf{3}^+$ is°the°most°stable ion° isomer° of° those° we° investigated° (Table° 1).° The optimized structure shows a planar ring and rather conventional lengths of the C—C, C—O, and C—N bonds°(Figure°3)°[5].°The°carbonyl-protonated°ion°($\mathbf{4}^+$) shows a conspicuously elongated O-1—C-2 bond (1.563 Å,° Figure° 3)° that° indicates° destabilization° of° the° oxazolone ring. The O-1—C-5 ring bond is completely broken (2.596 Å) in the O-1-protonated isomer $\mathbf{5}^+$ which shows a gauche geometry that can be described as an acylium cation that is weakly internally solvated with the°oxygen°atom°of°the°acetenolimine°group°(Figure°3). Ions $\mathbf{4}^+$ and $\mathbf{5}^+$ are substantially destabilized against $\mathbf{3}^+$ at all levels of theory, e.g., by 83 and 140 kJ mol^{-1}, respectively, according to CCSD(T)/6-311++G(3df,2p) calculations° (Table° 1).° Attempts° were° also° made° to obtain local energy minima for open-chain isomers of $\mathbf{3}^+$. However, regardless of the starting geometry, gradient optimizations including complete force constant analysis resulted in ring closure yielding $\mathbf{3}^+$. Hence we conclude that open-chain isomers of $\mathbf{3}^+$ are either inherently unstable or represent extremely shallow minima on the potential energy surface. Interestingly, Paizs et al. reported a high-energy, open-chain, gauche isomer for protonated 1,3-oxazol-5-one, but not for 2,3-dimethyl-° and° 2-isobutyloxazolones° [6].° Several conformers of another cyclic ion isomer, carbonyl-protonated N-acetylaziridinone ($\mathbf{6a}^+$-$\mathbf{6c}^+$), have been

Table 1. Ion relative and dissociation energies

Species/reaction	Energy[ab] 6-31++G(d,p) B3LYP	6-311++G(3df,2p) B3LYP	6-311++G(3df,2p) MP2	6-311++G(3df,2p) B3-MP2	6-311++G(3df,2p) CCSD(T)[c]
$\mathbf{3}^+$	0	0	0	0	0
$\mathbf{4}^+$	84	83	87	85	83
$\mathbf{5}^+$	152	143	135	139	140
$\mathbf{6a}^+$	222	221	226	223	229
$\mathbf{6b}^+$	227	225	228	226	232
$\mathbf{6c}^+$	239	236	238	237	242
$\mathbf{3}^+ \rightarrow CH_3CONH{=}CH_2^+ + CO$	113	108	114	111	97
$\mathbf{3}^+ \rightarrow CH_3CO^+ + NH{=}CH_2 + CO$	278	260	265	262	254
$\mathbf{3}^+ \rightarrow \mathbf{7}^{+\bullet} + H^\bullet$	396	391	391	391	401
$\mathbf{3}^+ \rightarrow \mathbf{1}^{+\bullet} + H^\bullet$	507	502	498	500	523
$\mathbf{3}^+ \rightarrow \mathbf{8}^{+\bullet} + H^\bullet$	423	409	413	411	434

[a]In units of kJ mol^{-1}.
[b]Including B3LYP/6-31++G(d,p) zero-point vibrational corrections and referring to 0 K.
[c]From basis set expansion according to eq 4.

found to be local energy minima. However, all these ion isomers are substantially less stable than $\mathbf{3}^+$ (Table 1).

We also report the dissociation energies of $\mathbf{3}^+$ (Table 1) to assess the energetics of the ion dissociations. Elimination of CO forming the *m/z* 72 ion is found to have the lowest thermochemical threshold at 97 kJ mol^{-1} relative to $\mathbf{3}^+$. This result is consistent with the dominant metastable-ion dissociation of $\mathbf{3}^+$. We note that Paizs et al. reported somewhat lower dissociation energies for loss of CO from protonated 1,3-oxazol-5-one and 2,3-dimethyl-1,3-oxazol-5-one at comparable levels of theory [6]. Consecutive dissociation by elimination of CO and CH_2 = NH to form CH_3CO^+ requires an additional 157 kJ mol^{-1} (Table 1). In contrast, loss of the methyl H-atom is a high-energy dissociation that requires 391 kJ mol^{-1} at the thermochemical threshold when forming the most stable 2-methylenoxazolin-5-one cation-radical $\mathbf{7}^{+\cdot}$. Losses of other hydrogen atoms from $\mathbf{3}^+$, e.g., from N-3 to form [2-methyl-1,3-oxazol-5-one]$^{+\cdot}$ ($\mathbf{1}^{+\cdot}$) or from C-4 to form [N-acetylaminoketene]$^{+\cdot}$ ($\mathbf{8}^{+\cdot}$), require even higher threshold energies (Table 1). The fact that loss of H occurs competitively with the other low-energy dissociations indicates involvement of electronically excited states of $\mathbf{3}^+$ upon collisional activation at 10 keV [35]. In summary, the major ion dissociations upon CAD of $\mathbf{3}^+$, as identified by isotope labeling, can be correlated with the relative energies of the products.

Neutralization-Reionization and Radical Dissociations

Collisional neutralization of $\mathbf{3}^+$ produces radical **3** whose NR mass spectrum is displayed in Figure 4. The spectrum shows extensive dissociations so that only a small fraction of surviving **3** is reionized and appears as survivor ions at *m/z* 100 (Figure 4a). Out of the several dissociation pathways observed, the most significant ones give rise to the products at *m/z* 99, 71, 57, 43, 42, 29, and 28. The products were identified with the help of deuterium labeling as illustrated by the NR mass spectra of **3a** and **3b** (Figure 4b,c). The loss of H from **3a** involves both light hydrogen and deuterium, as evidenced by the peaks at *m/z* 100 and 99. The loss of H or D from **3b** is difficult to distinguish because of a poorer signal to noise ratio in the spectrum. Nevertheless, it appears from the comparison of the Figure 3a and Figure 3b,c spectra that loss of D is hampered by kinetic isotope effects. The loss of 29 Da (*m/z* 71) shows a partial mass shift to *m/z* 72 (Figure 4b) and to *m/z* 73 (Figure 4c). An *m/z* 71 fragment is also present in the NR mass spectrum of $\mathbf{1}^{+\cdot}$ at [*m/z* 71]/[*m/z* 99] = 1.2. This indicates that the formation of the *m/z* 71 fragment from **3** involves consecutive dissociations by loss H and CO. The *m/z* 42 and 43 fragments show no retention of deuterium when formed from **3a** and **3b**, and hence must originate from the CH_3C—O moiety in **3**. The *m/z* 29 fragment shows only a partial 1 u shift to *m/z* 30 in the spectra of **3a** and **3b**, but no dominant shift to *m/z* 31 in the spectrum of the later radical. This indicates that the formation of the *m/z* 29 species (HCO, COH, or CH_2 = NH) is accompanied by H/D migrations. The NR mass spectra of **3**, **3a** and **3b** are dominated by the *m/z* 28 fragment. Deuterium labeling in **3a** and **3b** results in a partial shift to *m/z* 29. This indicates that the *m/z* 28 fragment is a mixture of CO and HCNH or CH_2 = N, with CO being the major component. This finding proves that upon electron-transfer, protonated oxazolones do dissociate by elimination of CO, invalidating one of the key arguments in the Haselmann hypothesis [9].

A few more minor features of the NR mass spectra deserve comments. Figure 3b and c show small but conspicuous peaks at *m/z* 86 and 87, respectively, that have no equivalent in the NR mass spectrum of **3**. We

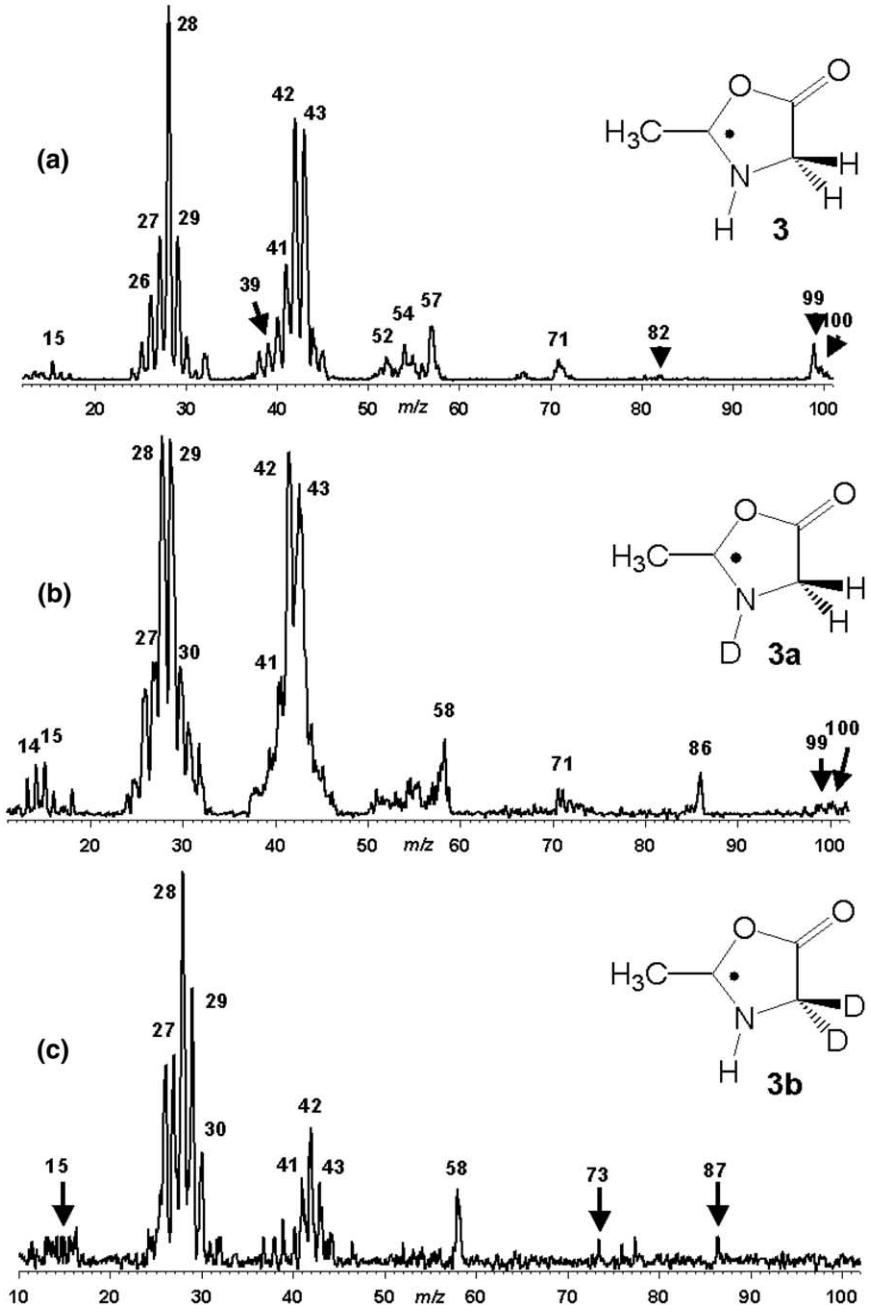

Figure 4. Neutralization (CH_3SSCH_3, 70%T)/reionization (O_2, 70%T) mass spectra of (**a**) $\mathbf{3}^+$, (**b**) $\mathbf{3a}^+$, and (**c**) $\mathbf{3b}^+$.

found by careful accurate mass measurements that the samples of **3a** and **3b** contained a trace amount of triethylamine that gave ions at *m/z* 101 ($M^{+\cdot}$) and *m/z* 102 $(M + H)^+$ amounting to about 5% of the $C_4H_5DNO_2$ and $C_4H_4D_2NO_2$ peaks from CI of **3a** and **3b**, respectively. It turned out that NR of the triethylamine ions was more efficient than that of $\mathbf{3a}^+$, $\mathbf{3b}^+$ and gave rise to a very abundant *m/z* 86 ion (Supplemental Material, Figure S1a) that contaminated the NR spectra of the labeled oxazolones. However, Figure S1b (Supplemental Material) shows that correcting for the contribution of triethylamine to eliminate the *m/z* 86 peak did not significantly affect the relative intensities of the other NR fragments from **3a**.

NR mass spectra of ions $\mathbf{3'}^+$ produced from N-acetylglycine ethyl ester were inconclusive because of mass interferences from dissociations of the adjacent and equally abundant *m/z* 99 ions. Because of fragment overlaps, the NR mass spectra of *m/z* 99 and *m/z* 100 precursor ions contained similar fragments when measured using the linked scan method and did not allow us to draw firm conclusions about the nature of **3′**. We note, however, that CAD spectra of $\mathbf{3'}^+$ that were interference free indicated that it and $\mathbf{3}^+$ were identically behaving ion species.

Table 2. Radical dissociation and transition state energies

Species/reaction	Energy[ab] 6-31++G(d,p) B3LYP	6-311++G(3df,2p) B3LYP	6-311++G(3df,2p) PMP2[c]	6-311++G(3df,2p) B3-PMP2[c]	6-311++G(3df,2p) CCSD(T)[d]
3	0	0	0	0	0
3 → **1** + H•	110	105	72	88	88
3 → **TS1**	119	118	107	113	117
3 → 7 + H•	172	160	137	148	153
3 → **8** + H•	194	178	166	172	186
3 → **TS2**	62	62	83	73	80
9	19	−20	−19	−19	−13
10	−17	−18	−16	−17	−10
3 → **TS3**	16	12	23	17	23
3 → **11** + CO	−5	−14	−6	−10	−10
3 → CO + $CH_3CO^•$ + $HN=CH_2$	127	114	134	124	119
3 → $CH_3CONH^•$ + $CH_2=C=O$	107	95	148	121	137
3 → CO + $CH_3CON=CH_2$ + H•	205	192	173	183	174
12	19	16	21	19	22
13	19	17	27	22	26
3 → **TS4**	130	132	153	142	136
3 → **TS5**	117	113	120	116	126
14	13	10	17	14	20

[a]In units of kJ mol^{-1}.
[b]Including B3LYP/6-31 ++ G(d,p) zero-point vibrational corrections and referring to 0 K.
[c]Spin-projected energies.
[d]From basis set expansion according to eq 4.

Radical Dissociation and Transition State Energies

To interpret the experimental data, we carried out ab initio calculations of the dissociation and transition-state energies of **3** and several relevant radical intermediates. The energies discussed in the text are all from ZPVE-corrected CCSD(T) single-point calculations, the energies calculated at the other levels of theory are listed in Table 2. The optimized radical structures are shown in Figure 5, the transition-state structures are in Figure 6, and the main dissociation pathways are visualized in a potential energy diagram in Figure 7.

Dissociation of the N-3—H bond in **3** requires 88 kJ mol^{-1} threshold energy to form 2-methyloxazol-5-one (**1**). As often observed for heteroatom—H bond dissociations in heterocyclic radicals, [24d, 24e, 36], the N-3—H bond dissociation requires an additional energy in the transition-state, E_{TS1} = 117 kJ mol^{-1} (Figure 7). Losses of other hydrogen atoms from **3** are substantially more endothermic. For example, a loss of an H atom from the methyl group forming 2-methylenoxazolin-5-one (**7**) requires 153 kJ mol^{-1} threshold energy, while a loss of an H atom from the C-4 methylene requires 186 kJ mol^{-1} to form N-acetylaminoketene (**8**) (Table 2).

Ring opening by breaking the O-1—C-5 bond requires the lowest transition-state energy at E_{TS2} = 80 kJ mol^{-1}. The open-ring radical **9** is 13 kJ mol^{-1} more stable than **3**, making the ring opening exothermic. Radical **9** can undergo a practically thermoneutral rotation about the C-4—C-5 bond to form an *anti*-rotamer **10**. Cleavage of the C-4—C-5 bond in **9** proceeds through a low-lying transition-state (TS3), E_{TS3} = 23 kJ mol^{-1} relative to **3**, to form CO and CH_3CO-NH-$CH_2^•$ (**11**) at -10 kJ mol^{-1} relative to **3**. Radical **11** can further dissociate by several low-energy pathways, e.g., by loss of H, $CH_2=C=O$, and $CH_2=NH$ (Table 2).

The alternative ring opening in **3** by cleavage of the N-3—C-4 bond is slightly endothermic when forming open-ring intermediates **12** and its rotamer **13**. The TS for this ring opening is at $E_{TS4} \approx$ 136 kJ mol^{-1} (Table 2) which is substantially higher than for the ring opening at O-1—C-5. We note that locating TS4 with B3LYP optimizations was difficult and not fully satisfactory, as the potential energy surface showed a cusp at *d*(N-3—C-4) ≈ 1.950 Å (Supplementary Material section, Figure S2). Thus, the TS4 energy from the present single-point calculations is rather tentative. Multireference CASSCF calculations including large active space (7 electrons, 12 orbitals) showed negligible mixing of other states at and near the TS4 geometry. The electron occupancies were as follows: singly-occupied molecular orbital (SOMO, 27): 1.00, doubly-occupied MO26: 1.92, MO25: 1.97, and MO24: 1.98, virtual orbitals MO28: 0.017, MO29: 0.0003, MO30: 0.0008, MO31: 0.022, MO32: 0.001, MO33: 0.005, MO34: 0.005, and MO35: 0.08. Hence, the problem with locating the TS was not due to an inadequate single-determinant wave function.

The unfavorable N-3—C-4 bond cleavage in **3** is probably due to stereoelectronic effects [37]. The oxazolone ring in **3** has a rigid near-planar conformation enforced by two sp^2 carbon atoms (C-2 and C-5).

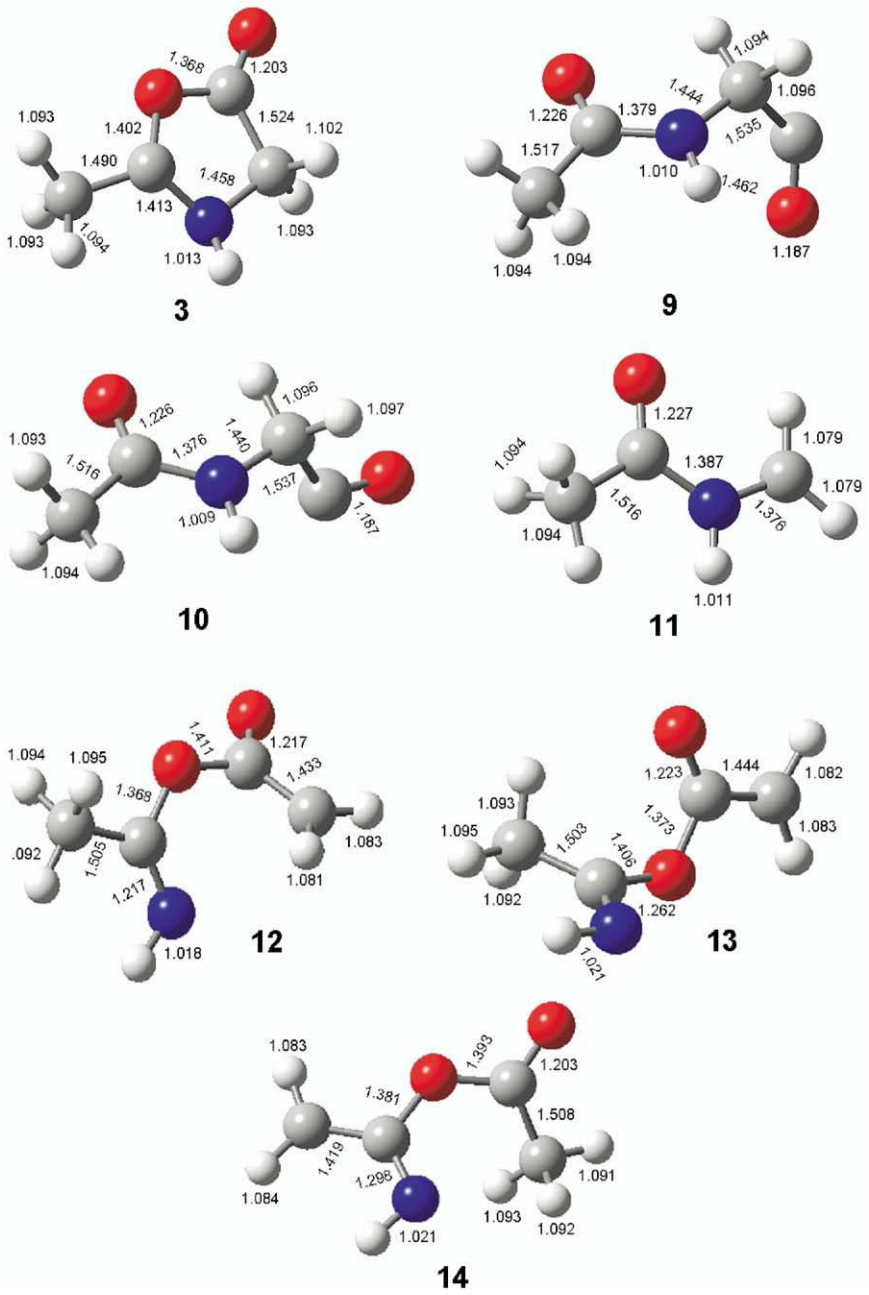

Figure 5. B3LYP/6-31 ++ G(d,p) optimized structures of radicals **3**, **9**–**14**. Bond lengths in angstroms.

In the course of N-3—C-4 bond dissociation the C-4 methylene group must rotate to assume the lowest energy conformation which is co-planar with the O-1—C-5 = O-6 group in the product **12** to allow electron delocalization over the CH_2—C(= O)—O—C = N system. However, such a rotation cannot take place in an early transition-state because of the ring rigidity, and the impaired electron delocalization contributes to the increased TS4 energy. Further reactions of intermediates **12** and **13** may involve elimination of ketene or an isomerization by intramolecular hydrogen transfer through **TS5** to form radical **14**, followed by loss of $CH_3CO^{\cdot}$. However, products of these dissociation pathways are *not* observed in the NR mass spectra of **3**, as established by deuterium labeling (vide supra), and thus must be kinetically disfavored.

In summarizing this part, the calculations indicate that a ring opening followed by CO expulsion is the *lowest-energy dissociation* of oxazolone radical **3**. The radical intermediates produced by CO loss can dissociate further to form CH_3CO, CH_2 = NH, and other low-mass fragments. These findings are in line with the experimental data from NR mass spectra.

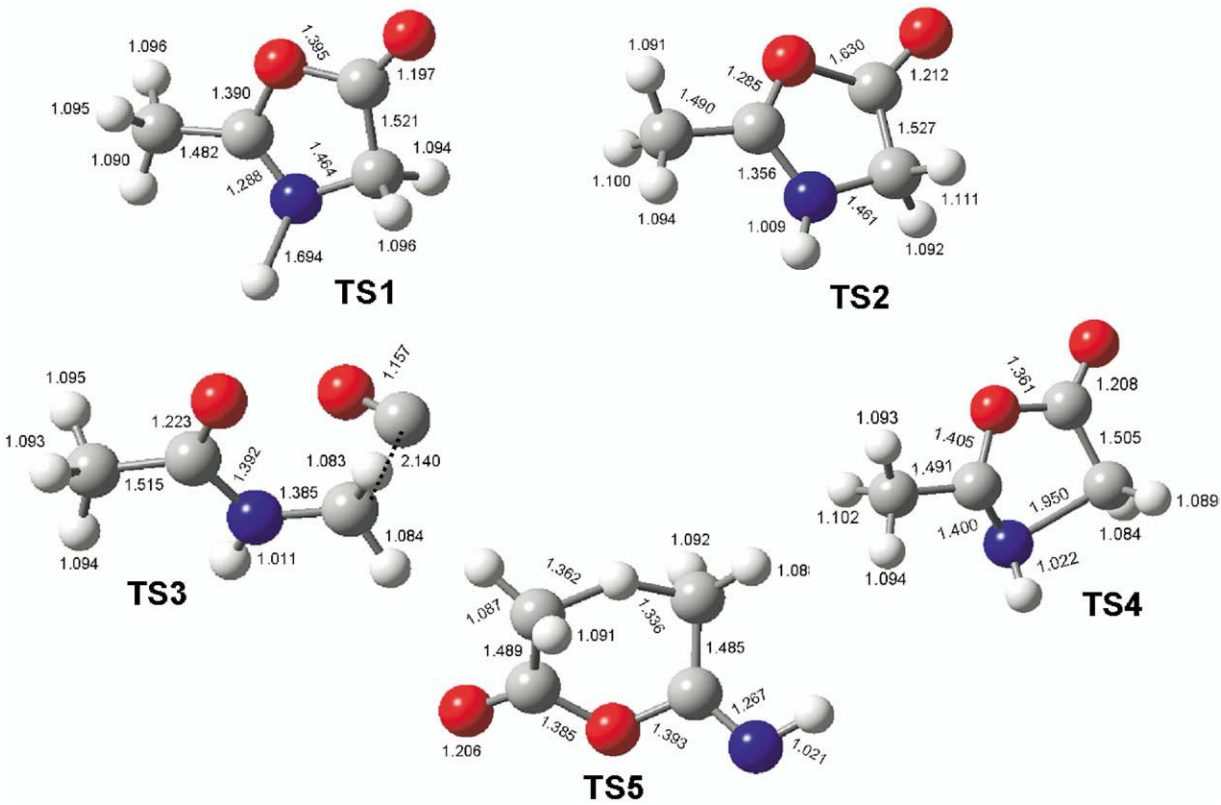

Figure 6. B3LYP/6-31 ++ G(d,p) optimized structures of transition states for radical isomerizations and dissociations. Bond lengths in angstroms.

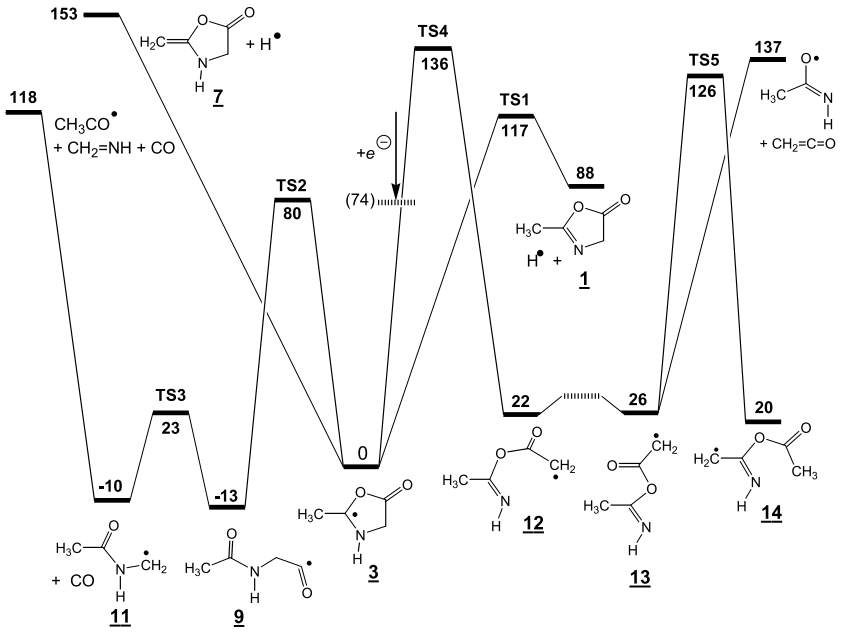

Figure 7. Potential energy diagram for dissociations of **3**. The energies are from single-point CCSD(T)/6-311 ++ G(3df,2p) calculations and include B3LYP/6-31 ++ G(d,p) ZPVE corrections.

Franck-Condon Effects

The NR mass spectra indicate extensive dissociation of **3** despite the fact that the radical is calculated to be inherently stable and reside in a 80 kJ mol^{-1} deep potential energy minimum. The reason for the rapid dissociation is the internal energy that the radicals receive upon collisional electron-transfer at keV kinetic energies [38]. Under these conditions, the radical internal energy consists of the precursor ion internal energy (E_{ion}), the electronic excitation (E_{exc}), and the excitation due to Franck-Condon effects (E_{FC}) [39,40]. E_{FC} ensue from a mismatch between the equilibrium geometry of the precursor cation and that of the radical, such that vertical electron-transfer results in vibrational excitation in the product [41]. The optimized geometries of $\mathbf{3}^+$ and **3** show major differences in the lengths of the O-1—C-2, C-2—N-3, O-1—C-5, and C-5—O-6 bonds (Figure 5). In addition, N-3 which is planar in $\mathbf{3}^+$ is pyramidized in **3**. These geometry differences can be expected to cause excitation of several stretching and bending vibrational modes in vertically produced **3**, e.g., the ν_{asym}(C-2—O-1—C-5) at 892 cm^{-1}, ν(O-1—C-5) at 1110 cm^{-1}, ν(C-3—N-3) at 1267 cm^{-1}, and ν(C-5—O-6) at 1799 cm^{-1}. The overall vibrational excitation in **3** due to Franck-Condon effects is calculated at 74 kJ mol^{-1}, close to the 80 kJ mol^{-1} TS energy for loss of CO.

Dissociation Kinetics and Branching Ratios

The transition-state energies were further used for RRKM calculations of unimolecular rate constants for dissociations of **3**. Figure 8 shows that the rate constant for the O-1—C-5 bond break reaches $k = 1/t = 2 \times 10^5$ s^{-1} within 4 kJ mol^{-1} of E_{TS2}, where t is the experimental time scale for radical dissociations (5.1 μs). This indicates that this dissociation of **3** is subject to a negligible kinetic shift in our measurements [42]. The consecutive dissociation by CO loss from intermediate **9** is very fast ($k > 10^{11}$ s^{-1}) at excitations achieved by crossing **TS2** in the preceding step. The reverse ring closure in **9** is 4 to 5 orders of magnitude slower than the loss of CO and does not affect the dissociation kinetics. The loss of H from N-3 shows a small kinetic shift of 20 kJ mol^{-1}. However, the loss of H from **3** is slower than the ring opening over the entire range of relevant internal energies. This is depicted in breakdown diagrams that were plotted using RRKM rate constants calculated at two levels of theory for dissociations occurring on the experimental time scale (Figure 9). In both cases, the loss of CO is predicted to account for >90% of dissociation over a broad range of internal energies.

A comparison of the calculated branching ratios with the product ion relative intensities in the NR mass spectra is not straightforward for several reasons. First, the ion intensities are affected by the cross sections for collisional reionization that tend to discriminate against small fragments [43]. Second, radical intermediates often undergo consecutive dissociations that result in convergent products formed by two or more dissociation pathways. Finally, the branching ratios from RRKM calculations usually describe dissociations on the potential energy surface of the ground electronic state, while NR mass spectra display dissociations from all electronic states accessed by collisional electron-transfer [44]. For these reasons, it is difficult to compare the extent of CO elimination in the NR mass spectra to the branching ratios from RRKM calculations.

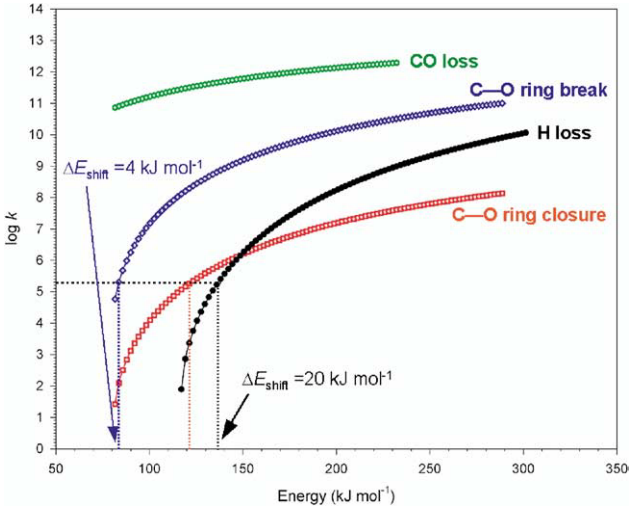

Figure 8. RRKM rate constants for unimolecular dissociations of **3**. ΔE_{shift} denotes the energy for the dissociation to occur with $k = 1/t$ on the experimental time scale t (the kinetic shift).

Ionization Energies and Excited Electronic States

The dissociations observed in the NR mass spectra may originate from any of the electronic states accessed by vertical electron-transfer. Figure 10 shows the recombination and ionization energies relevant to **3** and $\mathbf{3}^+$ and the three lowest excited electronic states in the radical. The adiabatic ionization energy of **3** (IE_{adiab} = 5.48 and 5.51 eV by CCSD(T) and B3-PMP2, respectively) is substantially different from both the vertical ionization energy, IE_{vert} = 6.94 eV, and the vertical recombination energy of $\mathbf{3}^+$, RE_{vert} = 4.70 eV. This indicates large Franck-Condon effects in both vertical neutralization and reionization. The first three electronically excited states of **3** (***A***-***C***) are within 1.80–2.62 eV (176-253 kJ mol^{-1}) of the ground state (***X***). If populated by collisional electron-transfer, these states can nonradiatively convert the electronic excitation energy into the vibrational energy of the ***X*** state of **3** and drive its primary and consecutive dissociations. Thus, involvement of even the lowest excited electronic states may explain the extensive dissociations of **3** upon collisional electron-transfer.

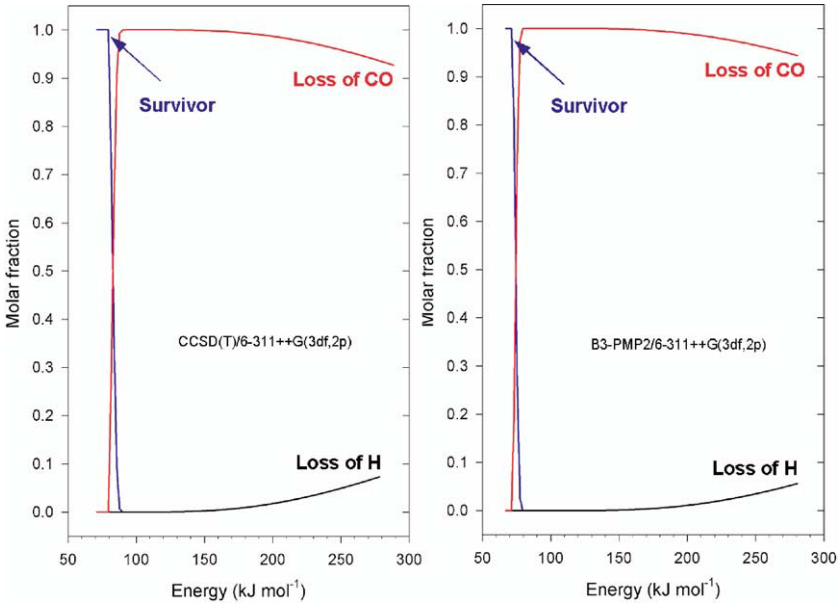

Figure 9. Calculated branching ratios for loss of H-3 and O-1—C-5 bond cleavage in **3**. Left panel: From CCSD(T)/6-311 ++ G(3df,3p) TS energies. Right panel: From B3-PMP2/6-311 ++ G(3df,2p) TS energies.

Discussion

The results of the present NR mass spectrometric measurements and energy and RRKM calculations are now used to discuss the properties of oxazolone radicals in connection with electron capture dissociation of ***b***-type ions. In their argumentation, Haselmann et al. presumed that oxazolone radicals should preferentially lose the amide hydrogen atom, not CO [9]. The present data clearly invalidate this argument by showing that loss of CO is in fact the dominating dissociation of oxazolone radicals. Another argument by Haselmann et

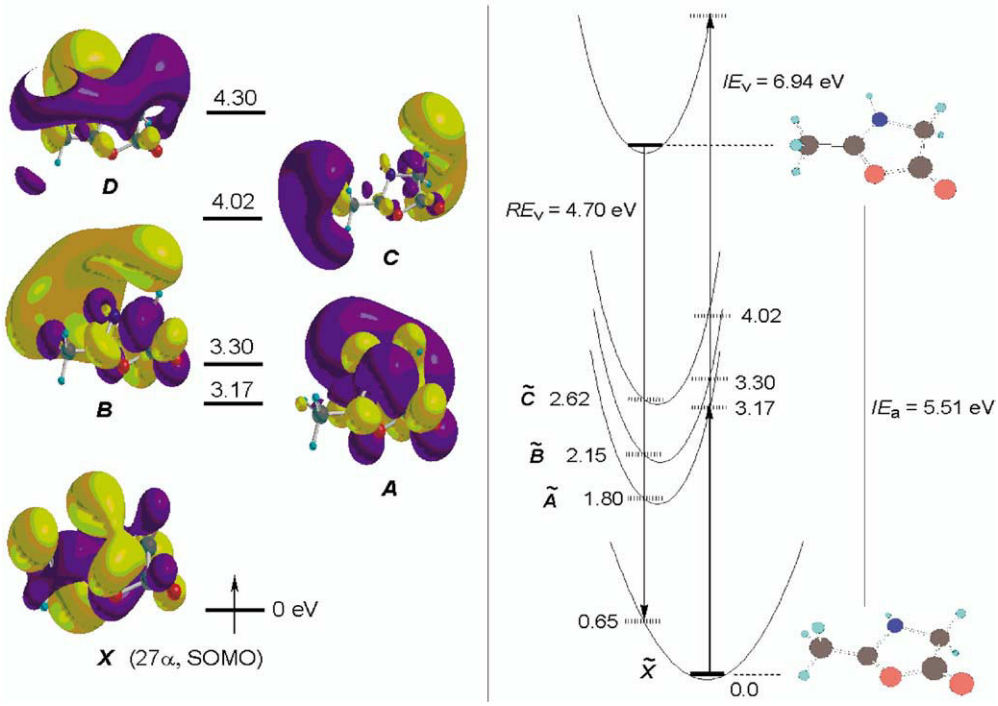

Figure 10. Left panel: Molecular orbitals for the ground (***X***) and ***A***–***D*** doublet excited states in **3**. Right panel: Ionization and excitation energies in **3** and recombination energies in $\mathbf{3}^+$. The vertical excitation energies are from TD-B3LYP/6-311 ++ G(2d,p) single-point calculations.

al. was that electron capture would not occur in a protonated oxazolone residue to drive the dissociation. The present data show that protonated oxazolones have recombination energies that are greater than those of protonated basic amino acid residues, e.g., guanidinium in Arg (3.53–3.56 eV) [45], ammonium in Lys (3.15–4.20 eV) [46] and imidazolium in His (3.55–3.87 eV) [47] There is a growing evidence from recent studies that ECD fragmentation of multiply charged peptides occurs at or near the charge sites of highest recombination energies[48]. According to this empirical rule, a protonated oxazolone residue in a doubly charged ***b***-ion should be the primary site of electron capture and the ensuing dissociation. Hence, both the electronic properties and the chemistry of oxazolone radicals, as revealed by the present study, are in keeping with the loss of CO upon ECD of ***b***-ions.

Conclusions

The present experimental and computational results show that oxazolone radicals formed by collisional electron-transfer undergo facile dissociation. The major dissociation pathway is exothermic ring opening by cleavage of the weak O-1—C-5 bond followed by elimination of CO and CH_3CO. Dissociations by H atom loss are less abundant and involve hydrogen atoms from both the ring and side-chain. These results lead us to conclude that oxazolone radicals are perfectly acceptable as intermediates of CO loss from ***b***-type peptide ions in electron capture dissociation. By refuting the arguments to the contrary, the present study supports cyclic oxazolone structures for gas-phase ***b***-ions from peptides.

Acknowledgments

The authors gratefully acknowledge support of this research by the National Science Foundation (grants CHE-0349595 for experiments and CHE-0342956 for computations). The Department of Chemistry Computational Facility was supported jointly by the NSF and University of Washington. Thanks are due to Dr. Martin Sadilek for assistance with CAD spectra measurements. The Jeol HX-110 mass spectrometer was a generous donation from the former Seattle Biomembrane Institute by courtesy of Professor S. Hakomori.

References

1. (a) Roepstorff, P.; Fohlmann, J. Proposal for a common nomenclature for sequence ions in mass spectra of peptides. *Biomed. Mass Spectrom.* **1984**, *11*, 601. (b) Biemann, K. Contributions of mass spectrometry to peptide and protein structure. *Biomed. Environ. Mass Spectrom.* **1988**, *16*, 99–111.
2. Papayannopoulos, I. A. The interpretation of collision-induced dissociation tandem mass spectra of peptides. *Mass Spectrom. Rev.* **1995,** *14,* 49–73.
3. Paizs, B.; Suhai, S. Fragmentation pathways of protonated peptides. *Mass Spectrom. Rev.* **2005,** *24,* 508–548.
4. Yalcin, T.; Khouw, C.; Csizmadia, I. G.; Peterson, M. R.; Harrison, A. G. Why are b ions stable species in peptide spectra? *J. Am. Soc. Mass Spectrom.* **1995,** *6,* 1165–1174.
5. Rodriquez, C. F.; Shoeib, T.; Chu, I. K.; Siu, K. W. M.; Hopkinson, A. C. Comparison between protonation, lithiation, and argentation of 5-oxazolones: A study of a key intermediate in gas-phase peptide sequencing. *J. Phys. Chem. A* **2000,** *104,* 5335–5342.
6. Paizs, B.; Szlavik, Z.; Lendvay, G.; Vekey, K.; Suhai, S. Formation of a_2^+ ions of protonated peptides. An ab initio study. *Rapid Commun. Mass Spectrom.* **2000,** *14,* 746–755.
7. (a) Csonka, I. P.; Paizs, B.; Lendvay, G.; Suhai, S. Proton mobility and main fragmentation pathways of protonated lysylglycine. *Rapid Commun. Mass Spectrom.* **2001**, *15*, 1457–1472. (b) Yalcin, T.; Harrison, A. G. Ion chemistry of protonated lysine derivatives. *J. Mass Spectrom.* **1996**, *31*, 1237–1243. (c) Farrugia, J. M.; O'Hair, R. A. J.; Reid, G. E. Do all b_2 ions have oxazolone structures? Multistage mass spectrometry and ab initio studies on protonated N-acylamino acid methyl ester model systems. *Int. J. Mass Spectrom.* **2001**, *210/211*, 71–87.
8. Nold, M. J.; Wesdemiotis, C.; Yalcin, T.; Harrison, A. G. Amide bond dissociation in protonated peptides. Structures of the N-terminal ionic and neutral fragments. *Int. J. Mass Spectrom. Ion Processes* **1997,** *164,* 137–153.
9. Haselmann, K. F.; Budnik, B. A.; Zubarev, R. A. Electron capture dissociation of b^{2+} peptide fragments reveals the presence of the acylium ion structure. *Rapid Commun. Mass Spectrom.* **2000,** *14,* 2242–2246.
10. (a) Danis, P. O.; Wesdemiotis, C.; McLafferty, F. W. Neutralization-reionization mass spectrometry (NRMS). *J. Am. Chem. Soc.* **1983**, *105*, 7454–7456. (b) Burgers, P. C.; Holmes, J. L.; Mommers, A. A.; Terlouw, J. K. Neutral products of ion fragmentations: HCN and HNC identified by collisionally induced dissociative ionization. *Chem. Phys. Lett.* **1983**, *102*, 1–3.
11. Holmes, J. L. The neutralization of organic cations. *Mass Spectrom. Rev.* **1989,** *8,* 513–539.
12. Tureček, F. The modern mass spectrometer. A chemical laboratory for unstable neutral species. *Org. Mass Spectrom.* **1992,** *27,* 1087–1097.
13. (a) Goldberg, N.; Schwarz, H. Neutralization-reionization mass spectrometry. A powerful laboratory to generate and probe elusive neutral molecules. *Acc. Chem. Res.* **1994,** *27,* 347–352. (b) Schalley, C. A.; Hornung, G.; Schröder, D.; Schwarz, H. Mass spectrometric approaches to the reactivity of transient neutrals. *Chem. Soc. Rev.* **1998,** *27,* 91–104. (c) Tureček, F. Transient intermediates of chemical reactions by neutralization-reionization mass spectrometry. *Top. Curr. Chem.* **2003,** *225,* 77–129.
14. (a) Sadilek, M.; Tureček, F. Probing hypervalent radicals by neutralization-laser photoionization mass spectrometry. *J. Phys. Chem.* **1996,** *100,* 9610–9614. (b) Polašek, M.; Tureček, F. Nitromethyl radical, cation, and anion. A neutralization and electron photodetachment-reionization mass spectrometric and ab initio computational study of $[C,H_2,N,O_2]$ isomers. *J. Phys. Chem. A* **2001,** *105,* 1371–1382. (c) Frank, A. J.; Tureček, F. Methylsulfonyl and methoxysulfinyl radicals and cations in the gas phase. A variable-time and photoexcitation neutralization-reionization and ab initio/RRKM study. *J. Phys. Chem. A* **1999,** *103,* 5348–5361.
15. (a) Kuhns, D. W.; Tran, T. B.; Shaffer, S. A.; Tureček, F. Methylthiomethyl radical. A variable-time neutralization-reionization and ab initio study. *J. Phys. Chem.* **1994,** *98,* 4845–4853. (b) Kuhns, D. W.; Tureček, F. Unimolecular neutral and ion kinetics by variable-time neutralization-reionization mass spectrometry. *Org. Mass Spectrom.* **1994,** *29,* 463–469. (c) Polašek, M.; Tureček, F. Direct observation of hydrogen atom adducts to nitromethane and methyl nitrite. A variable-time neutralization-reionization mass spectrometric and ab initio/RRKM study. *J. Phys. Chem. A* **1999,** *103,* 9241–9251. (d)

Sadilek, M.; Tureček, F. Dissociations of gas-phase CHClF and $CHCl_2$ radicals and cations following collisional electron transfer. A variable-time neutralization-reionization and ab initio study. *J. Phys. Chem.* **1996,** *100,* 224–232.
16. Gilbert, R. G.; Smith, S. C. Theory of unimolecular and recombination reactions; Blackwell: Oxford, 1990; pp 15–51
17. Kumar, P.; Mishra, H.; Mukerjee, A. K. Condensation of 2-substituted 5-oxo-4,5-dihydro-1,3-oxazoles with imines and their corresponding carbonyl compounds. *Synthesis* **1980,** 836–839.
18. Wieland, T.; Müller, R.; Niemann, E.; Birkofer, L.; Schöberl, A.; Wagner, A.; Söll, H. Stickstoffverbindungen III. Aminosäuren und ihre Derivate. In *Methoden der Organischen Chemie (Houben-Weyl); Müller, E., Ed.; Georg Thieme Verlag: Stuttgart,* 1958; pp 340–341.
19. Tureček, F.; Gu, M.; Shaffer, S. A. Novel tandem quadrupole acceleration-deceleration mass spectrometer for neutralization-reionization studies. *J. Am. Soc. Mass Spectrom.* **1992,** *3,* 493–501.
20. Frisch, M. J.; Trucks, G. W.; Schlegel, H. B.; Scuseria, G. E.; Robb, M. A.; Cheeseman, J. R.; Montgomery, J. A., Jr.; Vreven, T.; Kudin, K. N.; Burant, J. C.; Millam, J. M.; Iyengar, S. S.; Tomasi, J.; Barone, V.; Mennucci, B.; Cossi, M.; Scalmani, G.; Rega, N.; Petersson, G. A.; Nakatsuji, H.; Hada, M.; Ehara, M.; Toyota, K.; Fukuda, R.; Hasegawa, J.; Ishida, M.; Nakajima, T.; Honda, Y.; Kitao, O.; Nakai, H.; Klene, M.; Li, X.; Knox, J. E.; Hratchian, H. P.; Cross, J. B.; Adamo, C.; Jaramillo, J.; Gomperts, R.; Stratmann, R. E.; Yazyev, O.; Austin, A. J.; Cammi, R.; Pomelli, C.; Ochterski, J. W.; Ayala, P. Y.; Morokuma, K.; Voth, G. A.; Salvador, P.; Dannenberg, J. J.; Zakrzewski, V. G.; Dapprich, S.; Daniels, A. D.; Strain, M. C.; Farkas, O.; Malick, D. K.; Rabuck, A. D.; Raghavachari, K.; Foresman, J. B.; Ortiz, J. V.; Cui, Q.; Baboul, A. G.; Clifford, S.; Cioslowski, J.; Stefanov, B. B.; Liu, G.; Liashenko, A.; Piskorz, P.; Komaromi, I.; Martin, R. L.; Fox, D. J.; Keith, T.; Al-Laham, M. A.; Peng, C. Y.; Nanayakkara, A.; Challacombe, M.; Gill, P. M. W.; Johnson, B.; Chen, W.; Wong, M. W.; Gonzalez, C.; Pople, J. A. *Gaussian 03, Revision B.05*; Gaussian, Inc.: Pittsburgh, PA, 2003.
21. (a) Becke, A. D. A New mixing of Hartree-Fock and local-density-runcional theories. *J. Chem. Phys.* **1993,** *98,* 1372–1377. (b) Becke, A. D. Density functional thermochemistry. III. The role of exact exchange. *J. Chem. Phys.* **1993,** *98,* 5648–5652. (c) Stephens, P. J.; Devlin, F. J.; Chabalowski, C. F.; Frisch, M. J. Ab Initio calculation of vibrational absorption and circular dichroism spectra using density functional force fields. *J. Phys. Chem.* **1994,** *98,* 11623–11627.
22. Møller, C.; Plesset, M. S. Note on an approximation treatment for nano-electron systems. *Phys. Rev.* **1934,** *46,* 618–622.
23. (a) Schlegel, H. B. Potential energy curves using unrestricted Moeller-Plesset perturbation theory with spin annihilation. *J. Chem. Phys.* **1986,** *84,* 4530–4534. (b) Mayer, I. The spin-projected extended Hartree-Fock method. *Adv. Quantum Chem.* **1980,** *12,* 189–262.
24. (a) Tureček F. Proton affinity of dimethyl sulfoxide and relative stabilities of C_2H_6OS molecules and $C_2H_7OS^+$ ions. A comparative G2(MP2) ab initio and density functional theory study. *J. Phys. Chem. A* **1998,** *102,* 4703–4713. (b) Tureček, F.; Wolken, J. K. Dissociation energies and kinetics of aminopyrimidinium radicals by ab initio and density functional theory. *J. Phys. Chem. A* **1999,** *103,* 1905–1912. (c) Tureček, F.; Wolken, J. K.; Sadilek, M. Distinction of isomeric pyridyl cations and radicals by neutralization-reionization mass spectrometry, ab initio, and density functional theory calculations. *Eur. Mass Spectrom.* **1998,** *4,* 321–332. (d) Wolken, J. K.; Tureček, F. Heterocyclic radicals in the gas phase. An experimental and computational study of 3-hydroxypyridinium radicals and cations. *J. Am. Chem. Soc.* **1999,** *121,* 6010–6018. (e) Wolken, J. K.; Tureček, F. Modeling nucleobase radicals in the gas phase. Experimental and computational study of 2-hydroxypyridinium and 2(1H)-pyridone radicals. *J. Phys. Chem. A* **1999,** *103,* 6268–6281. (f) Tureček, F.; Carpenter, F. H. Glycine radicals in the gas phase. *J. Chem. Soc. Perkin Trans. 2* **1999,** 2315–2323. (g) Polašek, M.; Tureček, F. Hydrogen atom adducts to nitrobenzene: Formation of the phenylnitronic radical in the gas phase and energetics of Wheland intermediates. *J. Am. Chem. Soc.* **2000,** *122,* 9511–9524.
25. (a) Rablen, P. R. Is the acetate Anion stabilized by resonance or electrostatics? A systematic structural comparison. *J. Am. Chem. Soc.* **2000,** *122,* 357–368. (b) Rablen, P. R.; Bentrup, K. H. Are the enolates of amides and esters stabilized by electrostatics? *J. Am. Chem. Soc.* **2003,** *125,* 2142–2147.
26. Čížek. H.; Paldus, J.; Šroubková, L. Cluster expansion analysis for delocalized systems. *Int. J. Quantum. Chem.* **1969,** *3,* 149–167.
27. Purvis, G. D.; Bartlett, R. J. A full coupled-cluster singles and doubles model. The inclusion of disconnected triples. *J. Chem. Phys.* **1982,** *76,* 1910–1918.
28. Curtiss, L. A.; Raghavachari, K.; Pople, J. A. Gaussian-2 theory using reduced Møller-Plesset orders. *J. Chem. Phys.* **1993,** *98,* 1293–1298.
29. (a) Hegarty, D.; Robb, M. A. Application of unitary group methods for configuration interaction calculations. *Mol. Phys.* **1979,** *38,* 1795–1812. (b) Frisch, M.; Ragazos, I. N.; Robb, M. A.; Schlegel, H. B. An evaluation of three direct MC-SCF procedures. *Chem. Phys. Lett.* **1992,** *189,* 524–528.
30. Zhu, L.; Hase, W. L. *Quantum chemistry program exchange*; Indiana University: Bloomington, IN, 1994; Program no. QCPE 644.
31. Frank, A. J.; Sadilek, M.; Ferrier, J. G.; Tureček, F. Sulfur oxyacids and radicals in the gas phase. A variable-time neutralization-photoexcitation-reionization mass spectrometric and ab initio/RRKM study. *J. Am. Chem. Soc.* **1997,** *119,* 12343–12353.
32. NIST Standard reference database number 69; March, 2003; release; http://webbook.nist.gov/chemistry.
33. Bohme, D. K.; Mackay, G. I.; Schiff, H. I. Determination of proton affinities from the kinetics of proton transfer reactions. VII. The proton affinities of O_2, H2, Kr, O, N_2, Xe, CO_2, CH_4, N_2O, and CO. *J. Chem. Phys.* **1980,** *73,* 4976–4986.
34. Harrison, A. G. *Chemical Ionization Mass Spectrometry*, 2nd ed.; CRC Press: Boca Raton, 1992; p 18.
35. Chen, X.; Syrstad, E. A.; Gerbaux, P.; Nguyen, M. T.; Tureček, F. Distonic isomers and tautomers of adenine cation radical in the gas phase and aqueous solution. *J. Phys. Chem. A* **2004,** *108,* 9283–9293.
36. Wolken, J. K.; Tureček, F. Direct observation of a hydrogen atom adduct to O-4 in uracil. Energetics and kinetics of uracil radicals. *J. Phys. Chem. A* **2001,** *105,* 8352–8360.
37. (a) Tureček, F.; Hanuš, V. Stereoelectronic control of ion fragmentations. The loss of hydrogen from cyclic ethers during electron impact mass spectrometry. *Tetrahedron* **1983,** *39,* 1499–1506. (b) Tureček, F.; Pančíř, J.; Stahl, D.; Gäumann, T. Stereoelectronic effects on the retro-Diels-Alder fragmentation of ionized bicyclo[4.3.0]nona-3,7-dienes. *Org. Mass Spectrom.* **1985,** *20,* 360–367. (c) Tureček, F. Stereoelectronic effects in mass spectrometry. *Int. J. Mass Spectrom. Ion Processes* **1991,** *108,* 137–164.
38. Nguyen, V. Q.; Tureček, F. Energy effects in collisional neutralization with organic molecules. *J. Mass Spectrom.* **1996,** *31,* 843–854.
39. Tureček, F. The use of kinetic isotope effects for the determination of internal energy distributions of isolated transient species in the gas phase. *Int. J. Mass Spectrom.* **2003,** *227,* 327–338.

40. Hop, C. E. C. A.; Holmes, J. L. Fragmentation characteristics of the unstable $[CH_3CO]^{\cdot}$ radicals generated by neutralization of $[CH_3CO]^+$ cations. *Int. J. Mass Spectrom. Ion Processes* **1991,** *104,* 213–226.
41. (a) Tureček, F.; Gu, M.; Hop, C. E. C. A. Franck-Condon dominated chemistry. Formation and dissociations of tetrahydroxyphosphoranyl radicals following femtosecond reduction of their cations in the gas phase. *J. Phys. Chem.* **1995,** *99,* 2278–2291. (b) Nguyen, V. Q.; Shaffer, S. A.; Tureček, F.; Hop, C. E. C. A. Franck-Condon dominated chemistry. Dissociations of silicon-centered radicals prepared by femtosecond reduction of their cations in the gas phase. *J. Phys. Chem.* **1995,** *99,* 15454–15464.
42. Lifshitz, C. Time-resolved appearance energies, breakdown graphs, and mass spectra: The elusive kinetic shift. *Mass Spectrom. Rev.* **1982,** *1,* 309–348.
43. Hop, C. E. C. A.; Holmes, J. L. Neutralization-reionization mass spectrometry: Efficiency of the charge-exchange process. *Org. Mass Spectrom.* **1991,** *26,* 476–480.
44. Syrstad, E. A.; Vivekananda, S.; Tureček, F. Direct observation of a hydrogen atom adduct to C-5 in uracil. A neutralization-reionization mass spectrometric and ab initio study. *J. Phys. Chem. A* **2001,** *105,* 8339–8351.
45. Syrstad, E. A.; Tureček, F. Toward a general mechanism of electron-capture dissociation. *J. Am. Soc. Mass Spectrom.* **2005,** *16,* 208–224.
46. Tureček, F.; Syrstad, E. A. Mechanism and energetics of intramolecular hydrogen transfer in amide and peptide radicals and cation-radicals. *J. Am. Chem. Soc.* **2003,** *125,* 3353–3369.
47. Nguyen, V. Q.; Tureček, F. Protonation sites in gaseous pyrrole and imidazole: A neutralization-reionization and ab initio study. *J. Mass Spectrom.* **1996,** *31,* 1173–1184.
48. Iavarone, A. T.; Paech, K.; Williams, E. R. Effects of charge state and cationizing agent on the electron capture dissociation of a peptide. *Anal. Chem.* **2004,** *76,* 2231–2238.